An Approach to Minimize Aircraft Motion Bias in Multi-Hole Probe Wind Measurements made by Small Unmanned Aerial Systems

Loiy Al-Ghussain[1] and Sean C. C. Bailey[1]

[1]Department of Mechanical Engineering, University of Kentucky, Lexington, Kentucky, USA 40506

Correspondence: Sean Bailey (sean.bailey@uky.edu)

Abstract. Multi-hole probe mounted on an aircraft provide the air velocity vector relative to the aircraft, requiring knowledge of the aircraft spatial orientation (e.g. Euler angles), translational velocity, and angular velocity to translate this information to an Earth-based reference frame and determine the wind vector. As the relative velocity of the aircraft is typically an order of magnitude higher than the wind velocity, the extracted wind velocity is very sensitive to multiple sources of error including misalignment of the probe and aircraft coordinate system axes, sensor error and misalignment in time of the probe and aircraft orientation measurements in addition to aerodynamic distortion of the velocity field by the aircraft. Here, we present an approach which can be applied after a flight to identify and correct biases which may be introduced into the final wind measurement. The approach was validated using a ground reference, different aircraft, and for the same aircraft at different times. The results indicate significant reduction in wind velocity variance at frequencies which correspond to aircraft motion.

1 Introduction

The past few decades have witnessed significant increase in the utilization of small unmanned aerial systems (sUAS) in a wide range of atmospheric research areas, such as the evolution and structure of the atmospheric boundary layer (see, for example, van den Kroonenberg et al., 2007; Van den Kroonenberg et al., 2008; Cassano et al., 2010; Bonin et al., 2013; Lothon et al., 2014; Wildmann et al., 2015; Bärfuss et al., 2018; de Boer et al., 2018; Kral et al., 2018; Bailey et al., 2019), turbulence (Balsley et al., 2013; Witte et al., 2017; Bailey et al., 2019; Mansour et al., 2011; Calmer et al., 2018; Båserud et al., 2016), analysis of aerosols and gas concentration in the atmosphere (Bärfuss et al., 2018; Platis et al., 2016; Corrigan et al., 2008; Schuyler and Guzman, 2017; Illingworth et al., 2014; Zhou et al., 2018), cloud microphysics (Ramanathan et al., 2007; Roberts et al., 2008) and observation and analysis of extreme weather events such as hurricanes (Cione et al., 2016). This increasing interest in sUAS is motivated in part by the rapid increase in their commercial development and use combined with advantages of sUAS over traditional ground-based measurement systems utilizing either remote sensing or in situ approaches. Specifically, sUAS can acquire high spatial and temporal resolution measurements in a relatively low-cost package that provides flexibility in measurement location and flight path . In addition, when compared to manned aircraft measurements, their operation mitigates

risks associated with measurement at lower altitudes and during hazardous conditions or events (Elston et al., 2015; Bärfuss et al., 2018; Barbieri et al., 2019) such as erupted volcanoes with ash covers (Pieri et al., 2017), near thunderstorms (Elston et al., 2011) and over contaminated regions (Bärfuss et al., 2018).

The most common atmospheric properties sampled using sUAS are pressure, temperature, humidity and wind (e.g. Egger et al., 2002; Hobbs et al., 2002; Balsley et al., 2013; Witte et al., 2017; Bärfuss et al., 2018; Rautenberg et al., 2018; Jacob et al., 2018; Barbieri et al., 2019; Bailey et al., 2019). Although these scalar quantities are relatively straightforward to acquire, obtaining all three components of the wind velocity vector is complicated by the presence of the continual translation and rotation of the measurement platform, resulting in different approaches developed to determine the wind vector (Rautenberg et al., 2018; Suomi and Vihma, 2018; Laurence and Argrow, 2018; Shevchenko et al., 2016). Wind velocity measurements typically can be partitioned into several approaches: directly by using the instrumentation employing an on-board wind sensor and subtract the aircraft kinematics (Suomi and Vihma, 2018; Cassano et al., 2016); indirectly using the attitude and position data recorded by the inertial measurement unit (IMU) and GPS, respectively (Suomi and Vihma, 2018); using both techniques (Rautenberg et al., 2018); or through calibration of the aircraft's kinematic and dynamic response to the wind (González-Rocha et al., 2020).

Broadly speaking, wind measurements taken by sensors like sonic anemometers, single- and multi-hole pressure probes, and hot-wires tend to have higher temporal (and hence spatial) response (Suomi and Vihma, 2018). Multi-hole pressure probes have been frequently used for sUAS-based wind velocity measurements (Van den Kroonenberg et al., 2008; Elston et al., 2015; Spiess et al., 2007; Thomas et al., 2012) due to their high sampling frequency, light weight, simplicity, accuracy and almost linear relation between pressure and velocity at large flow velocities (Suomi and Vihma, 2018). More importantly, multi-hole probes are able to resolve all three wind velocity components. The simplest multi-hole probe capable of resolving all three velocity components is the five-hole probe, composed of five holes arranged symmetrically on a semi-spherical or conical tip. When the wind velocity is oriented in different directions relative to the probe axis, each hole converts a different proportion of the dynamic pressure to stagnation pressure, allowing the dynamic pressure and direction to be determined using laboratory or in-flight calibration of the probe's directional response.

The use of five-hole probes in sUAS measurements has evolved from their employment in manned aircraft measurements (Lenschow, 1970, 1972). Such measurements frequently employ in-flight calibration procedures. For instance, Parameswaran and Jategaonkar (2004) presented the calibration procedure of five-hole probes using flight recorder data using an optimization algorithm to estimate the time delay, biases and scale factors in the pressure measurements. Afterwards, the corrected five-hole probe measurements were compared with the measurements from the inertial measurement unit to check their compatibility. Drüe and Heinemann (2013) present a comprehensive review of in-flight calibration of several atmospheric measurement instruments, including five-hole probes. They identified five-hole probe in-flight calibration maneuvers to determine the sideslip angle, angle of attack, static pressure and position errors. Moreover, they highlighted the need for in-flight calibration in the experiment location under favorable atmospheric conditions and following removal of the sensors from the aircraft.

The simplicity and compact nature of multi-hole probes also make it particularly useful for fixed-wing sUAS. However, as with manned aircraft, these aircraft have the ability to fly at velocities up to an order of magnitude greater than the wind

velocity, their usage can be very sensitive to small errors in calibration and probe alignment (Suomi and Vihma, 2018; Laurence and Argrow, 2018). Furthermore, accurate position and orientation determination usually requires very accurate orientation information (e.g. obtained through the use of dual-antenna combination GPS/IMU units) and accurate time-stamping of the data is critical to align sensor and and flight data. Here, we present an approach which can be implemented *a posteriori* to minimize the impact of unidentified and unquantified biases introduced during wind velocity measurement which result in contamination of the wind signal by the aircraft velocity. This contamination results in over- or under- estimation of the wind vector and, in particular, errors in estimation of turbulence statistics (e.g. momentum fluxes, dissipation rate, turbulence kinetic energy) measured by the sUAS. Hence, it is vital to minimize errors in the wind components measured by sUAS. In the following sections we overview a multi-hole probe implementation and discuss the potential sources of bias within the approach. We then present a simple automated optimization which is designed to identify and remove these biases and demonstrate that this approach improves the wind estimate of an existing dataset.

2 Multi-hole Probe Implementation

Multi-hole probes are an adaptation of the common Pitot-static probe to allow the determination of relative wind direction as well as magnitude. Widely used in laboratory wind-tunnel studies of three-dimensional flow fields, they found use in manned-aircraft studies of atmospheric wind (Treaster and Yocum, 1978; Axford, 1968; Lenschow, 1972) before being adopted for sUAS use. Five-hole probes, being the simplest form of multi-hole probes, are most common. The arrangement of the normal vector of each plane of the holes on the probe tip typically consists of a central hole with normal vector in line with the probe axis, measuring pressure P_1, and with the normal vector of the remaining holes at an angle to the probe axis. Two holes measure the pressure at opposing directions on the horizontal plane e.g. P_2 and P_3, with the remaining two on opposite directions on the vertical plane, e.g. P_4 and P_5. Static pressure, P_s is also measured, either through a ring of holes oriented perpendicular to the probe axis, or through an alternate pressure port. Wind tunnel calibrations are used to determine calibration coefficients, for example

$$C_{P_{yaw}} = (P_2 - P_3)/(P_1 - \overline{P}) \tag{1}$$

$$C_{P_{pitch}} = (P_2 - P_5)/(P_1 - \overline{P}) \tag{2}$$

$$C_{P_{total}} = (P_1 - P_0)/(P_1 - \overline{P}) \tag{3}$$

$$\overline{P} = (P_2 + P_3 + P_4 + P_5)/4, \tag{4}$$

where $P_0 = 0.5\rho|\boldsymbol{U}_m|^2 + P_s$ is the total pressure, ρ the density of the air and $|\boldsymbol{U}_m|$ the magnitude of the relative air velocity vector $\boldsymbol{U}_m$. During calibration P_1, P_2, P_3, P_4, P_5 and P_s are measured at different sideslip, β, and angle of attack, α, angles at known P_0. Depending on the specifics of the probe geometry, a unique set of coefficients is recovered for each α and β combination up to some limit (referred to as the cone angle) typically between $25°$ and $45°$ depending on the specifics of the probe geometry. During measurement P_1, P_2, P_3, P_4, P_5 and P_s are simultaneously sampled and $C_{P_{yaw}}$, $C_{P_{pitch}}$ calculated for each sample. The known dependence of α, β and $C_{P_{total}}$ on $C_{P_{yaw}}$, $C_{P_{pitch}}$ from the calibration is then applied to determine α,

β and P_0 which, when combined with a known ρ, provides the air velocity and direction relative to the probe axis. Additional calibration is also possible to account for imprecise frequency response of the probes caused by resonance and viscous damping in the pressure tubing and sensors (e.g. as described in Gerstoft and Hansen (1987)) which can potentially require additional corrections (e.g. Yang et al., 2006). These additional corrections are not addressed here.

95   When implemented on a moving platform such as an aircraft, U_m is no longer the wind velocity but is instead a combination of the aircraft and wind velocity vectors

$$[U_m]_B = [U]_B - [U_s]_B \tag{5}$$

where U_s is the velocity vector of the sensor and U is the desired wind velocity vector. We have also introduced the subscript B to indicate that these velocities are in a body-fixed frame of reference, i.e. a coordinate system attached to the aircraft. Due to

100   the pitch, roll and yaw angles of the aircraft, $\Omega = [\theta \, \phi \, \gamma]$, or more specifically their time rate of change $\dot{\Omega}$, U_s can experience additional velocity relative to the aircraft velocity $U_{ac} = [U_{ac} \, V_{ac} \, W_{ac}]$ (Lenschow and Johnson, 1968) such that

$$[U_s]_B = [U_{ac}]_B + [\dot{\Omega} \times r]_B \tag{6}$$

where r is the distance vector between the aircraft center of gravity and the measurement volume on the probe.

Note that the desired quantity is $[U]_I = [U \, V \, W]$, the wind velocity vector in the Earth-fixed inertial frame of reference.

105   Furthermore, U_{ac} is also typically measured in the Earth-fixed inertial frame (e.g. through global positioning system) and therefore a transformation matrix L_{BI} must be determined using the aircraft's pitch (θ), roll (ϕ), and yaw (γ) angles in the inertial frame. The velocity vector $[U_{ac}]_I$ along with θ, ϕ, γ and their rates as required to build Ω and L_{BI} can be measured by an on-board inertial measurement unit and GPS, and are commonly provided by most autopilots used for sUAS operation. Thus, providing enough information to determine $[U]_I$ from $[U_m]_B$.

110   However, as noted earlier, U_s is often an order of magnitude larger than the desired U, making the process sensitive to an abundance of small biases. For example, the procedure above assumes perfect alignment between the probe's coordinate system and the aircraft's coordinate system. It also assumes that the Ω and L_{BI} are measured at the aircraft's center of gravity; that r is precisely known; that there are negligible flow blockage effects in the wind tunnel calibration or from the aircraft fuselage; and that all sensors are free of error. Although every effort can be made to minimize these biases, it is unlikely that

115   they can be removed completely. The result is that U often contaminated by U_s. This is most evident when L_{BI}, U_{ac} and Ω are changing rapidly. The following section describes a procedure developed to determine additional calibration coefficients and implement them following an in-flight calibration or measurement to minimize these biases.

3   Correction procedure

The net effect of the majority of biases can be summarized as influencing four parameters. Misalignment of probe and aircraft

120   axes, calibration errors, and aerodynamic distortion of the flow around the probe will introduce bias errors into the time-dependent pitch, roll and yaw angles $\theta(t)$, $\phi(t)$ and $\gamma(t)$, which relate the measured velocity vector in body-frame coordinates

to the aircraft velocity vector. In addition, calibration errors, transducer errors, and airframe aerodynamic effects (e.g. airframe blockage and streamline deflection due to the generation of lift) can also influence the direction of airflow relative to the probe as well as the magnitude of the measured dynamic pressure $Q(t) = 0.5\rho(t)|\boldsymbol{U}_m(t)|^2$ relative to the true dynamic pressure.

125 Note that the distortion of the flow may also depend on lift production of the aircraft and therefore $Q(t)$ may also include dependence on lift coefficient, which is not considered in the version of the corrections described here. Finally, it is also important for all sensor readings to precisely correspond to orientation readings in time to allow precise removal of aircraft motion from measured relative air velocity. However, implementation of software and differences in sensor time response can cause a delay between when probe measured velocity and aircraft measured velocity occur, e.g. the values of $\boldsymbol{U}_m(t)$ and $\boldsymbol{U}_s(t)$

130 may not correspond to the same t. The proposed correction procedure assumes that these values are biased in a way such that

$$\theta(t) = \theta_m(t) + \Delta\theta \tag{7}$$

$$\phi(t) = \phi_m(t) + \Delta\phi \tag{8}$$

$$\gamma(t) = \gamma_m(t) + \Delta\gamma \tag{9}$$

$$Q(t) = \zeta\, Q_m(t) \tag{10}$$

135 $$\boldsymbol{U}_m(t) = \boldsymbol{U}_m(t_m + \Delta t) \tag{11}$$

where the subscripted m indicates the measured value. The objective is then to find $\Delta\epsilon = \{\Delta\theta,\, \Delta\phi,\, \Delta\gamma,\, \zeta,\, \Delta t\}$. Using assumptions about how these biases will impact $\boldsymbol{U}(t)$ allows the determination of optimal values for $\Delta\epsilon$ which minimize this negative behavior. With $\Delta\epsilon$ known, we are able to remove its influence on the final time-series of $\boldsymbol{U}(t)$.

The assumptions used here are relatively straightforward. The first being that any biasing of $\boldsymbol{U}(t)$ by $\boldsymbol{U}_s$ will result in $\boldsymbol{U}(t)$

140 having dependence on the direction of travel of the aircraft. The second assumption we make is that the vertical component of $\boldsymbol{U}(t)$ will be approximately zero in the mean. This assumption may not hold in flight over sloped terrain or/and for relatively short flight domains (both spatial and temporal) , in which case an alternative assumption may be needed. Moreover, we assume that the sensors have adequate response and the greatest error due to the specific configuration which logs IMU/GPS, pressure transducers, and PTU on three separate systems.

145 The correction procedure, as implemented, follows a multistage approach used to optimize $\Delta\epsilon$. This multistage approach was implemented to allow different objective functions to be used for different components of $\Delta\epsilon$. However, in practice, it is likely that a well-implemented single-stage optimization will achieve the same results.

The first step is to identify a portion of the flight which will be used to determine $\Delta\epsilon$. This portion should not include any significant acceleration or deceleration of the aircraft's horizontal ground speed (e.g. as experienced during takeoff or landing)

150 and should include multiple changes of direction of the aircraft. In addition, the portion should be long enough to ensure that unsteadiness in the mean winds, e.g. as introduced by thermals, are averaged out. Ideally, devoting a portion of the flight after takeoff to conduct calibration orbits for later use in this process would be desired. With this portion of flight identified, the determination of $\Delta\epsilon$ is found by an optimization process seeking to minimize an objective function, δ, through iterative calculation of $[\boldsymbol{U}]_I$ (as described in Section 2).

155 Through perturbing $\Delta\epsilon$ and examining its influence on $\boldsymbol{U}(t)$ it was found that the standard deviation of the horizontal components of $[\boldsymbol{U}(t)]_I$, specifically $U(t)$ and $V(t)$, were most sensitive to Δt (due to the aircraft flight being predominantly in the horizontal plane) with values of Δt as low as tenths or hundredths of a second contributing to large biases of the horizontal components of $[\boldsymbol{U}(t)]_I$. We thus first use a Nelder-Mead multidimensional unconstrained nonlinear minimization approach, implemented using the Matlab *fminsearch* command, to identify the value of Δt which minimizes the objective function δ,

160 defined as

$$\delta_U = \langle U\rangle|_{U_{ac}>0} - \langle U\rangle|_{U_{ac}<0} \tag{12}$$

$$\delta_V = \langle V\rangle|_{U_{ac}>0} - \langle V\rangle|_{U_{ac}<0} \tag{13}$$

$$\delta = \delta_U^2 + \delta_V^2. \tag{14}$$

Note that $\langle\ \rangle|_{U_{ac}>0}$ indicates an average conditioned on when the aircraft is flying with positive inertial velocity component U_{ac}.

165 Likewise $\langle\ \rangle|_{U_{ac}<0}$ indicates an average of all values obtained when the aircraft inertial U_{ac} velocity component is negative. The selection of U_{ac} vs V_{ac} for conditioning is arbitrary, and should be selected based on the actual flight trajectory flown. For flight trajectories without many trajectory changes, it was also found that the objective function

$$\delta = \langle(U - \langle U\rangle)^2\rangle + \langle(V - \langle V\rangle)^2\rangle \tag{15}$$

was equally effective, but relies on the assumption that the biases will act only to increase the fluctuations of the velocity signal

170 at the probe. Here $\langle\ \rangle$ indicates an average over the entire portion of the flight used to find $\Delta\epsilon$. The resulting value of Δt which minimizes δ is then implemented in the remaining optimization stages.

  The second stage follows a similar approach. Noting that the mean value of the vertical component of $[\boldsymbol{U}(t)]_I$, i.e. $W(t)$, is most sensitive to $\Delta\theta$, we then find the value of $\Delta\theta$ that minimizes

$$\delta = \langle W\rangle \tag{16}$$

175 using $\boldsymbol{U}_m(t) = \boldsymbol{U}_m(t_m + \Delta t)$ as found above.

  The remaining elements of $\Delta\epsilon$, specifically ζ, $\Delta\phi$ and $\Delta\gamma$, are then found by minimizing δ as defined in Equation 14 using $\boldsymbol{U}_m(t) = \boldsymbol{U}_m(t_m + \Delta t)$ and $\theta = \theta_m + \Delta\theta$ as found in the preceding two stages.

  Finally, to ensure that the values of $\Delta\epsilon$ determined using the latter optimization stages do not influence the values found during the earlier stages, $\Delta\epsilon$ is further refined by repeating the above three stages once again. In practice, this last step only

180 influenced $\Delta\epsilon$ by one percent or less and likely can be omitted without loss of confidence in the final values of $\Delta\epsilon$.

4 Results

With $\Delta\epsilon$ known, the biases described by $\Delta\epsilon$ can be removed following Equations 7 to 11 prior to a final determination of $[\boldsymbol{U}(t)]_I$. To validate this correction procedure, we applied it to measurement data acquired during the LAPSE-RATE campaign described in de Boer et al. (2018). The data was acquired using two different five-hole-probe-equipped fixed-wing aircraft, with

185   the aircraft, probe, and data reduction procedures described in detail in Witte et al. (2017). We first demonstrate the correction procedure in flights compared to a ground reference, followed by a demonstration of the improvements made to vertical profiles of the wind velocity and direction.

4.1   Comparison to ground reference

A key part of the LAPSE-RATE campaign was an intercomparison study between numerous sUAS measuring pressure, tem-

190   perature, humidity, wind speed and wind direction. As detailed in Barbieri et al. (2019), the intercomparison was conducted by flying the sUAS near the Mobile UAS Research Collaboratory (MURC) vehicle, which was equipped with a 15 m mast supporting reference instruments, including a sonic anemometer. For the fixed-wing aircraft used here, this comparison was performed by having the aircraft orbit the mast at 20 m above ground level with an orbit radius of 80 m. This orbit was performed for approximately 5 minutes before the aircraft ascended to 120 m to perform similar orbits for 2 minutes, then

195   descending back to 20 m to resume the orbits around the tower for another 2 minutes before starting its landing pattern.

This circular flight pattern introduced a periodic variation in θ, γ and ϕ, with the period corresponding to the time to complete an orbit (approximately 25 s). Although convenient for the measurement of atmospheric parameters at a single geographic location, these types of orbits consist of the worst-case scenario for the contamination of the measured wind direction by the biases discussed in Section 2.

200   The periodicity is clearly evident in the estimated horizontal wind speed, $V_h = (U^2 + V^2)^{1/2}$, and direction, ψ, prior to implementing the corrections, as shown in Fig. 1a and 1b respectively. Although the general trends of the measured wind velocity and direction time series follow that of the reference velocity and direction, the magnitude of the fluctuations are clearly contaminated by the aircraft velocity and direction. The period in the wind signal is consistent with the time required to orbit the fixed mast at 25 s. Note that in Fig. 1 only the two portions of the flight where the sUAS is at the same altitude as

205   the reference sensors are presented.

The same time series are shown in Figs. 2a and 2b corrected following the procedure described in Section 3. The ten minutes of flight between 12:49 MDT and 12:58 MDT were selected to conduct the optimization of $\Delta\epsilon$. The the result of optimization was $\Delta\epsilon = \{\Delta\theta = -6.4°, \Delta\phi = 0.9°, \Delta\gamma = 2.1°, \zeta = 1.07, \Delta t = -0.045s\}$ which highlights the sensitivity of the estimated wind velocity and direction to even small deviations from ideal orientations. As shown in Fig. 2. The corrected signals are now

210   largely free of the 25 s periodicity, although there is some evidence of contamination between 12:56 MDT and 12:58 MDT. When the aircraft returns to 18 m altitude for the second set of orbits (which were not included in the optimization) there is little evidence of aircraft velocity contamination in the wind estimates.

The periodicity described above is more clearly evident in the difference between the power spectrum of horizontal wind speed calculated for both the corrected and uncorrected cases. These spectra are presented in Fig.3. The influence of the

215   periodic orbits of the aircraft is apparent in the uncorrected measurements as a spike at 0.035 Hz (consistent with an orbital period of 28 s). This spike is greatly reduced by the correction. Importantly, besides what appears to be a harmonic peak at 0.07 Hz which is also reduced, the remainder of the spectrum appears largely unaffected by the correction.
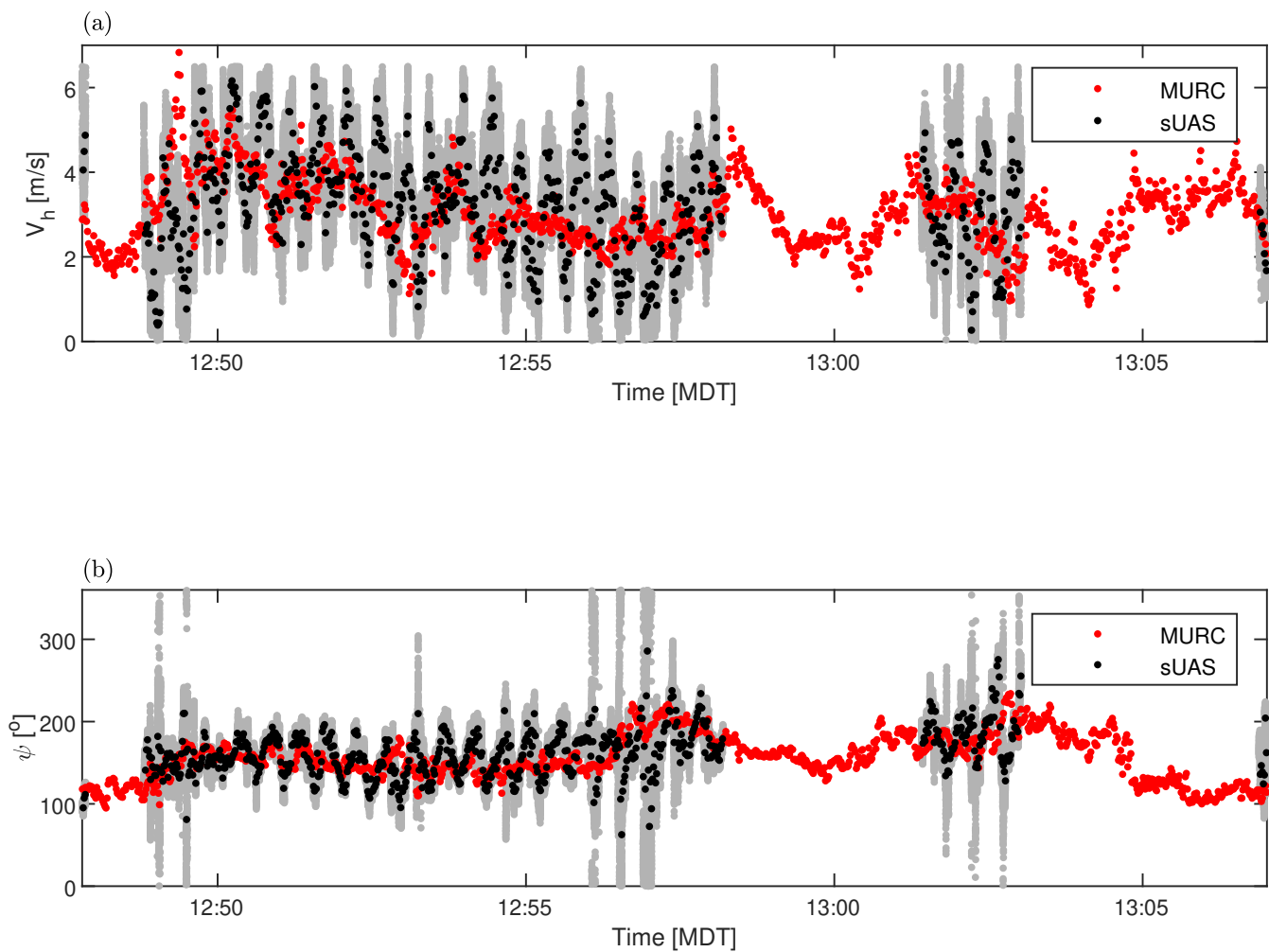
Figure 1. Comparison between uncorrected (a) horizontal wind speed and (b) wind direction measured by sUAS to the reference signal measured by MURC. Gray lines indicate full signal from sUAS, whereas black lines indicate same signal downsampled to same data rate as that of the MURC by plotting every 200th data point .
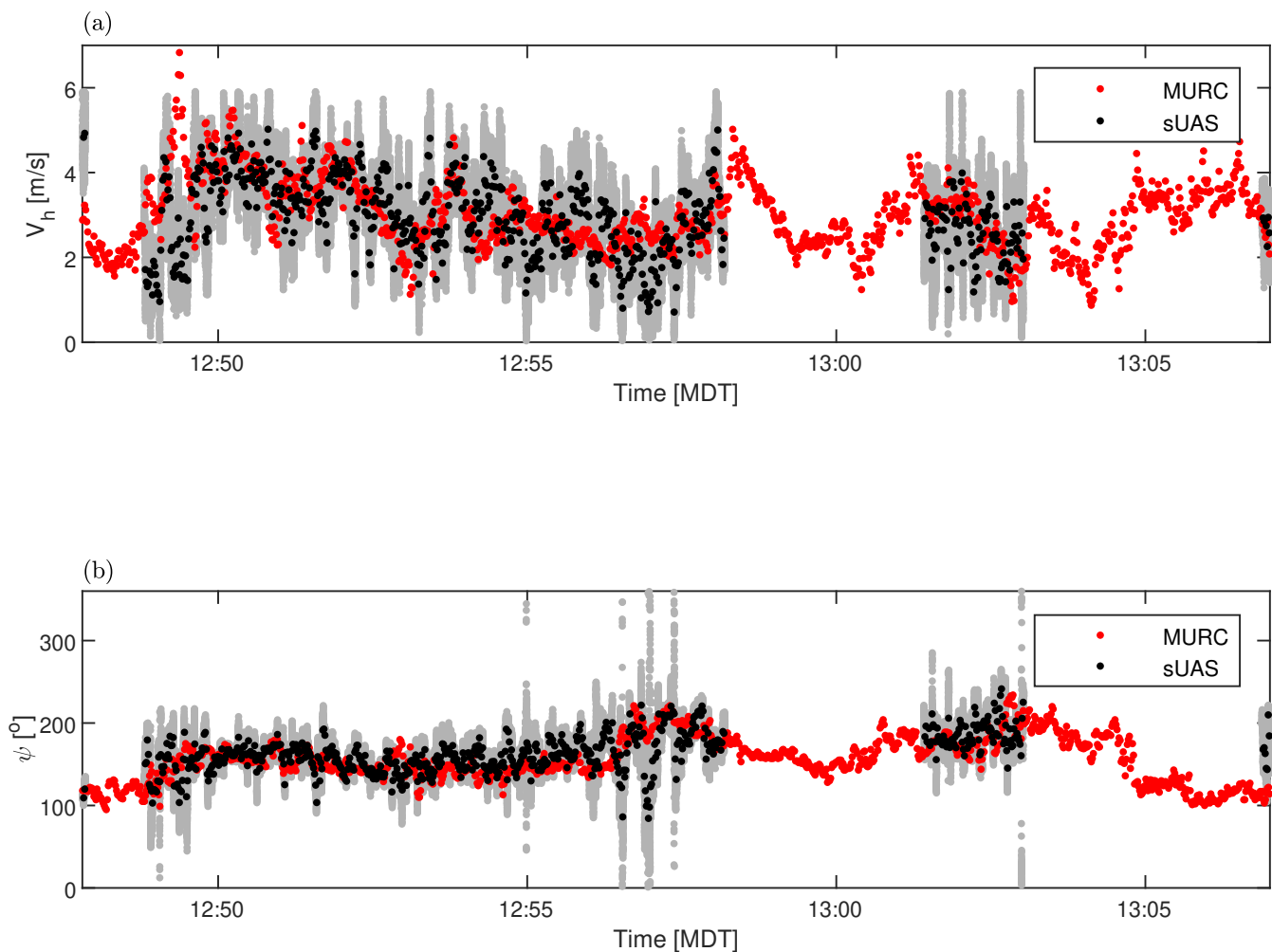
Figure 2. Small unmanned aerial system-based wind measurements from Fig. 1 following correction compared to the reference signal measured by MURC: (a) horizontal wind speed and (b) wind direction. Gray lines indicate full signal from sUAS, whereas black lines indicate same signal downsampled to same data rate as that of the MURC by plotting every 200th data point .
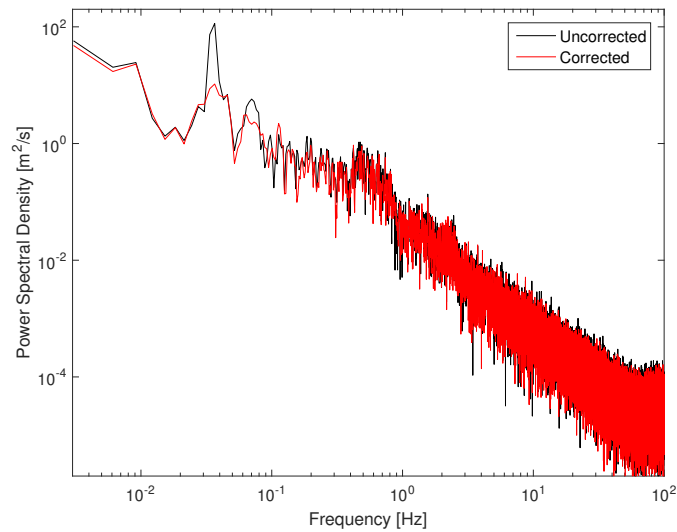
Figure 3. Power spectrum of horizontal wind magnitude calculated from uncorrected and corrected time series

To provide a more quantitative comparison between the sUAS and reference measurement, we directly compare the velocity magnitude and direction measured at each instant a sample was made by the ground reference. This comparison is presented in Fig. 4 in which a perfect comparison would result in the straight line as indicated on these figures. Note that, a perfect correlation should not be expected as the sUAS and reference sensor were not collocated. Also shown as a dashed line on these figures are the bounds described by 2 standard deviations of the difference between the sUAS and MURC measured values.

For the uncorrected velocity magnitude and direction, the comparison shown in Figs. 4a and 4b reveals a broad spread about the reference line. This spread decreases significantly when the corrections are applied, as shown by comparison to Figs. 4c and 4d. The mean difference between the two measurements decreases by approximately 35% in magnitude and direction with correction, corresponding to an increase in the correlation coefficient from 0.13 to 0.19 in magnitude and 0.22 to 0.32 in direction. This increased correlation is reflected in the statistics. The correction brings the standard deviation of the sUAS measured velocity much closer to the reference signal. The standard deviation in magnitude measured by the sUAS decreases from 1.2 m/s to 0.90 m/s, very close to the value of 0.86 m/s measured by the reference. For direction the standard deviation decreases with correction from $27°$ to $22°$ whereas it is $24°$ for the reference.

4.2 Implementation in profiling measurements

The results of the comparison to the ground reference provide confidence in the success of the correction. To demonstrate the improvement offered by application of these corrections on vertical profiling by fixed-wing aircraft, we now examine their impact on profiles of wind speed and direction measured by two separate aircraft at different locations. These two fixed-wing aircraft were essentially identical in configuration to that described in Witte et al. (2017) and were flown at measurement sites
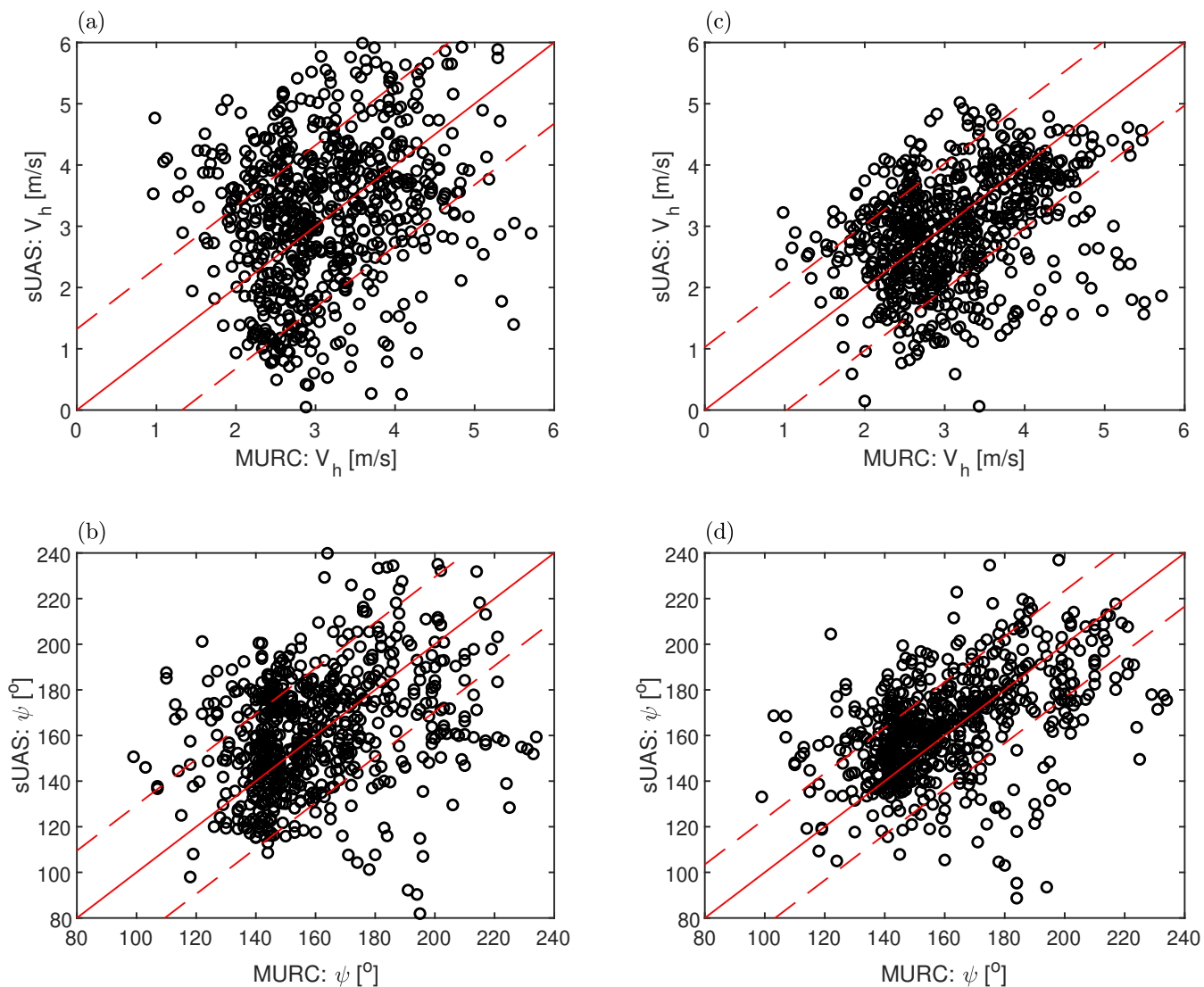
Figure 4. Direct comparison between (a) uncorrected and (c) corrected horizontal wind speed measured simultaneously by sUAS and MURC. Similar comparison shown for (b) uncorrected and (d) corrected wind direction. Solid red line indicates line where both measurements identical and dashed lines indicate 2 standard deviations of the difference between the sUAS and MURC measured values.

separated by 16 km. Each aircraft measured an atmospheric profile every hour, with the two aircraft staggered in time by 30 minutes.

Each profile consisted of a 20 minute flight, with the aircraft performing a spiralling ascent to 900 m followed by a spiralling descent, with this pattern repeated until the 10Ah battery was expended. In the following discussion the times are those corresponding to when the profile measuring flight initiates with the X, Y, Z coordinate system's origin at the takeoff location. These particular profiles were selected for discussion as they were measured during the boundary layer transition, and represent different behaviors, including the presence of turbulence and variability in the wind direction. The wind speeds during these profiles were also low, producing a large ratio of aircraft velocity to wind velocity and therefore a challenging case to accurately extract the wind components from the five-hole-probe signal.

As previously mentioned, the orbital flight patterns also represented a challenge for extracting the wind data due to the periodic variation in θ, γ and ϕ introducing a corresponding periodic variation in $[\boldsymbol{U}(t)]_I$. This bias can be clearly illustrated by comparing γ to ψ, as done for an example flight in Fig. 5a. For this flight, the aircraft completed a full 360° turn in approximately 30 s, introducing a corresponding period in both the wind speed and direction before correction. Once the corrections have been applied, as shown in Fig. 5b, there is a distinct reduction of periodicity in the direction of the wind measured by the sUAS.

The mean of the corresponding wind speed and direction profiles are presented in Fig. 6 for sUAS 1 and Fig. 7 for sUAS 2. In these figures both the uncorrected and corrected mean profiles are displayed in order to show the relative improvement offered by application of the bias correction. For all profiling flights, the correction coefficients were determined by optimizing the entire flight once the aircraft was in its flight pattern. Before correction, the bias introduced by the aircraft trajectory is apparent as large coherent deviations from the general trend, mostly evident in the velocity magnitude, but also present in the direction. When the corrections were applied, these large deviations were greatly reduced, better representing the structure of the boundary layer throughout the profiles. In the wind velocity profiles presented in Fig. 6 for sUAS 1 there were still high velocity deviations, even in the corrected profiles near the surface corresponding to when the aircraft was being manually controlled and experiencing strong accelerations. It has been found that the corrections presented here cannot completely remove the bias due to aircraft acceleration, suggesting a potential time response lag between the five-hole probe and the inertial measurement unit which agrees with what was reported in (Båserud et al., 2016) .

The corrected profiles show very different wind behaviors existed for the different sites and times. At the site measured by sUAS 1, the profiles measured at 8:30 MDT and shown in Figs. 6a,b reflect the correspondence between the stable thermodynamic conditions throughout the boundary layer and the horizontal wind magnitude, with winds increasing from 2 m/s near the ground to 4 m/s at $Z = 900$ m and consistently between $\psi = 0°$ and $100°$. There was noticeably stronger velocity and direction fluctuations measured for $Z < 200$ m, indicating the presence of turbulence near the surface. This turbulence appears to have been still present at 9:30 MDT, as shown in Figs. 6c,d, but at this time there was a region of calm air centered at $Z = 600$ m, coinciding to a significant deviation in measured wind direction. For $Z > 200$ m, the corrected profile of wind direction was consistent with the one measured at 8:30 MDT, excepting the region of calm air at $Z = 600$ m.
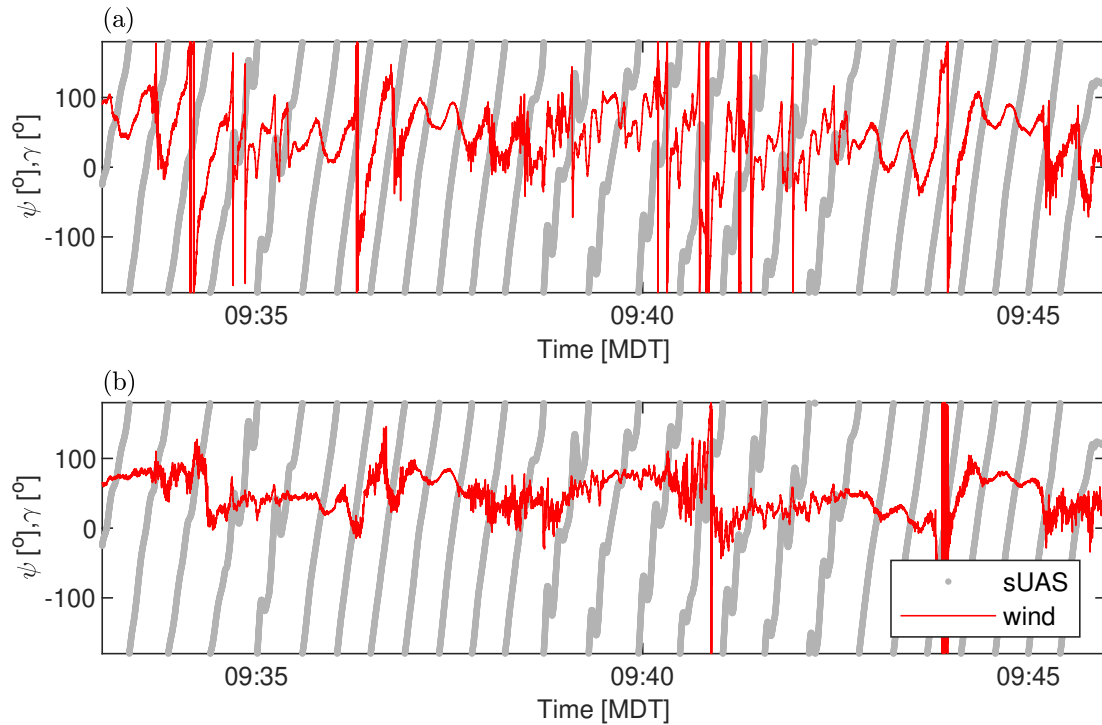
Figure 5. Comparison between measured wind direction and aircraft yaw direction for (a) uncorrected and (b) corrected signals as a function of time for a single flight.

At the site measured by sUAS 2, the corrected mean wind speed and direction profiles measured at 9:10 MDT and shown in Figs. 7a,b reflect a boundary layer undergoing transition, with evidence of turbulence for $Z < 500$ m. At 10:10 MDT, as shown in Figs. 7c,d, a multi-layer structure was also evident in the wind profiles in the form of significant changes in the wind direction throughout the profile. The horizontal wind speed was relatively consistent between 1 to 2 m/s for $Z < 800$ m, but there was evidence of stronger turbulence for $Z < 500$ m and moderate wind shear for $Z > 700$ m. As noted, the wind direction exhibited significant variation in the range 400 m$< Z < 500$ m, with continual backing within 500 m$< Z < 900$ m, and veering for $Z < 900$ m. These different altitudes of behavior were consistent with the measured potential temperature changes (not included for conciseness), and became much easier to identify in the corrected profiles than they were before correction.

It is clear through comparison of the corrected and uncorrected profiles in Figs. 6 and 7 that the corrections reduce fluctuations about the mean profile under different conditions and for different aircraft. Similar improvements have been observed for other profiles measured with these and other sUAS. The coefficients determined by the optimization routine for these profiles are presented in Table 1. Comparing each flight by the same sUAS demonstrates that the automated optimization converged on nearly identical coefficients for the same sUAS with only one coefficient changing by more than $1°$ between each flight. Indeed,
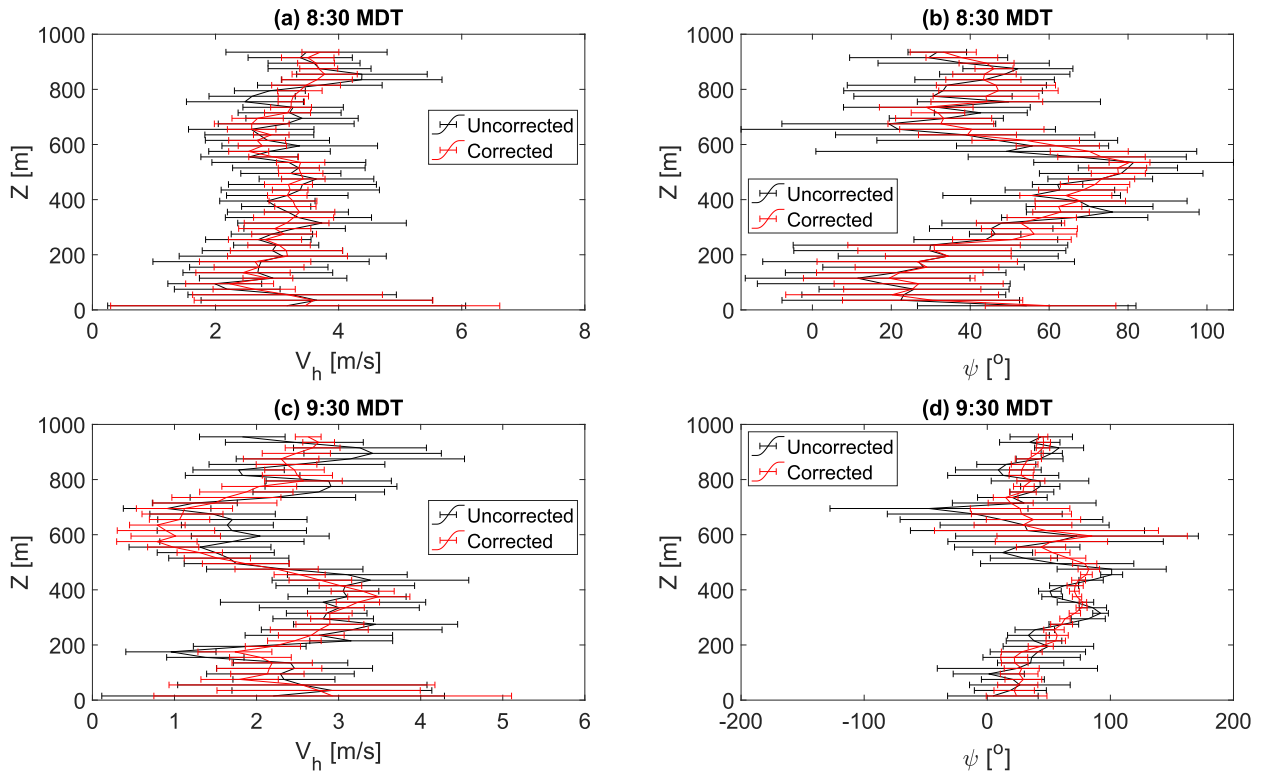
Figure 6. Comparison of mean (a) horizontal wind magnitude and (b) wind direction profiles measured by sUAS 1 at 8:30 MDT with and without correction applied. Horizontal mean magnitude and direction profiles measured at 9:30 MDT shown in (c) and (d) respectively.

sUAS	Flight	$\Delta\theta$	$\Delta\phi$	$\Delta\gamma$	ζ	Δt
1	8:30 MDT	$-4.9°$	$0.17°$	$2.6°$	1.1	0.98 s
1	9:30 MDT	$-5.8°$	$2.7°$	$2.1°$	1.1	0.01 s
2	9:10 MDT	$-3.9°$	$0.85°$	$1.4°$	1.15	2.9 s
2	10:10 MDT	$-3.9°$	$0.78°$	$1.3°$	1.15	2.6 s

Table 1. Components of $\Delta\epsilon$ determined by optimization for each sUAS for both flights.
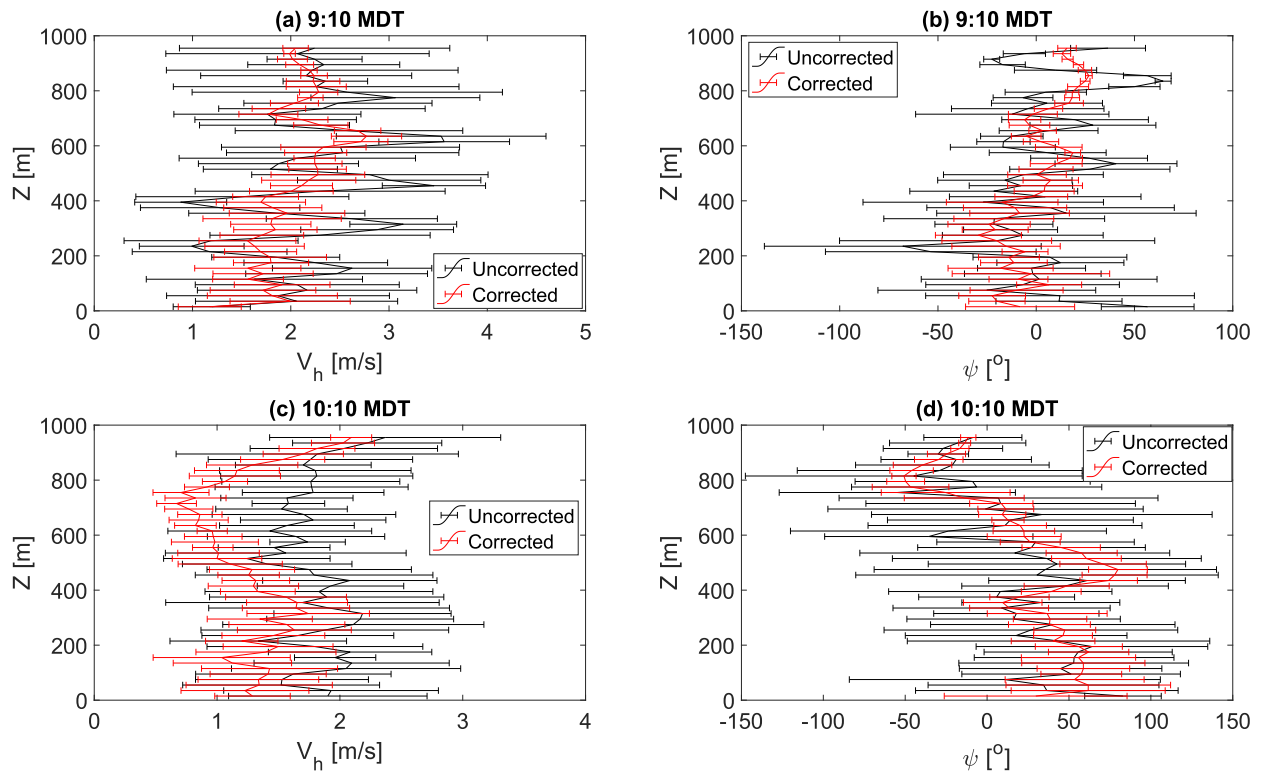
Figure 7. Comparison of mean (a) horizontal wind speed and (b) direction profiles measured by sUAS 2 at 9:10 MDT with and without correction applied. Horizontal wind speed and direction profiles measured at 10:10 MDT shown in (c) and (d) respectively.

the correction coefficients were found to be remarkably similar for each sUAS used throughout the LAPSE-RATE campaign.
This similarity between the coefficients reinforces the assumption that the biases are caused by physical misalignment between the coordinate systems of the aircraft and five-hole probe. Note that bias corrected by Δt should not be expected to be consistent for the systems used here, as the time series of $\boldsymbol{U}_m$, $\boldsymbol{U}_{ac}$ and $\boldsymbol{\Omega}$ are measured by separate acquisition systems at different rates and aligned using post-processing software. Thus the Δt bias is most likely introduced by errors in this alignment process and can be expected to be random.

5 Conclusions

Small unmanned aerial systems have been increasingly used in atmospheric research. Frequently, this research requires the acquisition of the wind velocity vector. Multi-hole probe measurements are among the more common and reliable techniques used for this purpose. However, when implemented on sUAS there is significant potential to introduce bias due to the large ratio of aircraft velocity to the wind velocity. Therefore, the measured wind velocities are very sensitive to these small biases.

295 Furthermore, when conducting vertical profiles at a fixed location, these profiles typically require circular flight patterns which increase the probability of small misalignment between the probe and the aircraft axes introducing a time-dependent, periodic error in the wind velocity measurement that can propagate into post-flight analysis such as the calculation of energy spectra and Reynolds stresses.

An approach was presented that can be applied in post-processing of the flight data to automatically estimate the biases in

300 axis misalignment, as well as errors in their alignment in time. Once estimated, these biases can be removed, improving the quality of the wind estimate.

These corrections were validated using data acquired as part of the LAPSE-RATE field campaign. Measurements flown near a ground-based reference system revealed significant reduction in measured oscillations of both wind magnitude and direction, which corresponded to the aircraft flight pattern. Additional verification was conducted by comparing profiles of

305 wind speed and direction measured by two different aircraft at two different times. The estimated biases were within $\pm 1°$ for each aircraft, and successful minimization of aircraft-induced oscillations in the measured profiles was observed for both aircraft. These results confirm that the biases are most likely due to physical misalignment of the aircraft and probe axes, as well as demonstrating that the same correction procedures can be applied to multiple aircraft.

Author contributions. S.B. conceived the correction, which was implemented by L.A-G. Both authors contributed to manuscript preparation.

310 *Competing interests.* The authors declare no competing interests are present.

Acknowledgements. This work was supported by the National Science Foundation through grant #CBET-1351411 and by the National Science Foundation Award No.1539070, Collaboration Leading Operational UAS Development for Meteorology and Atmospheric Physics (CLOUDMAP). The authors would like to thank Caleb Canter, Jess Estridge, Jonathan Hamilton, Sean MacPhee, Ryan Nolin, Isaac Rowe, Christopher Saunders, Virginia Smith, Christina Vezzi and Harrison Wight who maintained and flew the aircraft used in this study, as well as

315 calibrated and manufactured the probes.

References

Axford, D. N.: On the Accuracy of Wind Measurements Using an Inertial Platform in an Aircraft, and an Example of a Measurement of the Vertical Mesostructure of the Atmosphere, Journal of Applied Meteorology, 7, 645–666, https://doi.org/10.1175/1520-0450(1968)007<0645:OTAOWM>2.0.CO;2, 1968.

320 Bailey, S. C. C., Canter, C. A., Sama, M. P., Houston, A. L., and Smith, S. W.: Unmanned aerial vehicles reveal the impact of a total solar eclipse on the atmospheric surface layer, Proceedings of the Royal Society A: Mathematical, Physical and Engineering Sciences, 475, 20190 212, https://doi.org/10.1098/rspa.2019.0212, https://royalsocietypublishing.org/doi/abs/10.1098/rspa.2019.0212, 2019.

Balsley, B. B., Lawrence, D. A., Woodman, R. F., and Fritts, D. C.: Fine-scale characteristics of temperature, wind, and turbulence in the lower atmosphere (0–1,300 m) over the south Peruvian coast, Boundary-Layer Meteorology, 147, 165–178, 2013.

325 Barbieri, L. et al.: Small Unmanned Aircraft Systems (sUAS) in Atmospheric Science: Measurement Intercomparison for LAPSE-RATE, Sensors (in review), 2019.

Bärfuss, K., Pätzold, F., Altstädter, B., Kathe, E., Nowak, S., Bretschneider, L., Bestmann, U., and Lampert, A.: New setup of the UAS ALADINA for measuring boundary layer properties, atmospheric particles and solar radiation, Atmosphere, 9, https://doi.org/10.3390/atmos9010028, 2018.

330 Båserud, L., Reuder, J., Jonassen, M. O., Kral, S. T., Paskyabi, M. B., and Lothon, M.: Proof of concept for turbulence measurements with the RPAS SUMO during the BLLAST campaign, Atmospheric Measurement Techniques Discussions, pp. 1–22, https://doi.org/10.5194/amt-2015-407, 2016.

Bonin, T., Chilson, P., Zielke, B., and Fedorovich, E.: Observations of the Early Evening Boundary-Layer Transition Using a Small Unmanned Aerial System, Boundary-Layer Meteorology, 146, 119–132, https://doi.org/10.1007/s10546-012-9760-3, http://dx.doi.org/10.1007/s10546-012-9760-3, 2013.

335

Calmer, R., Roberts, G. C., Preissler, J., Sanchez, K. J., Derrien, S., and O'Dowd, C.: Vertical wind velocity measurements using a five-hole probe with remotely piloted aircraft to study aerosol-cloud interactions, Atmospheric Measurement Techniques, 11, 2583–2599, https://doi.org/10.5194/amt-11-2583-2018, 2018.

Cassano, J. J., Maslanik, J. A., Zappa, C. J., Gordon, A. L., Cullather, R. I., and Knuth, S. L.: Observations of Antarctic polynya with
340 unmanned aircraft systems, Eos, Transactions American Geophysical Union, 91, 245–246, 2010.

Cassano, J. J., Seefeldt, M. W., Palo, S., Knuth, S. L., Bradley, A. C., Herrman, P. D., Kernebone, P. A., and Logan, N. J.: Observations of the atmosphere and surface state over Terra Nova Bay, Antarctica, using unmanned aerial systems, Earth System Science Data, 8, 115–126, https://doi.org/10.5194/essd-8-115-2016, 2016.

Cione, J., Kalina, E., Uhlhorn, E., Farber, A., and Damiano, B.: Coyote unmanned aircraft system observations in Hurricane Edouard (2014),
345 Earth and Space Science, 3, 370–380, 2016.

Corrigan, C., Roberts, G., Ramana, M., Kim, D., and Ramanathan, V.: Capturing vertical profiles of aerosols and black carbon over the Indian Ocean using autonomous unmanned aerial vehicles, Atmospheric Chemistry and Physics, 8, 737–747, 2008.

de Boer, G., Ivey, M., Schmid, B., Lawrence, D., Dexheimer, D., Mei, F., Hubbe, J., Bendure, A., Hardesty, J., Shupe, M. D., McComiskey, A., Telg, H., Schmitt, C., Matrosov, S. Y., Brooks, I., Creamean, J., Solomon, A., Turner, D. D., Williams, C., Maahn, M., Argrow, B., Palo,
350 S., Long, C. N., Gao, R.-S., and Mather, J.: A Bird's-Eye View: Development of an Operational ARM Unmanned Aerial Capability for Atmospheric Research in Arctic Alaska, Bulletin of the American Meteorological Society, 99, 1197–1212, https://doi.org/10.1175/BAMS-D-17-0156.1, https://doi.org/10.1175/BAMS-D-17-0156.1, 2018.

Drüe, C. and Heinemann, G.: A review and practical guide to in-flight calibration for aircraft turbulence sensors, Journal of Atmospheric and Oceanic Technology, 30, 2820–2837, https://doi.org/10.1175/JTECH-D-12-00103.1, 2013.

355   Egger, J., Bajrachaya, S., Heingrich, R., Kolb, P., Lammlein, S., Mech, M., Reuder, J., Schäper, W., Shakya, P., Shween, J., and H., W.: Diurnal Winds in the Himalayan Kali Gandaki Valley. Part III: Remotely Piloted Aircraft Soundings, Mon. Wea. Rev., 130, 2042–2058, 2002.

Elston, J., Argrow, B., Frew, E., Houston, A., and Straka, J.: Evaluation of unmanned aircraft systems for severe storm sampling using hardware-in-the-loop simulations, Journal of Aerospace Computing, Information, and Communication, 8, 269–294, 2011.

360   Elston, J., Argrow, B., Stachura, M., Weibel, D., Lawrence, D., and Pope, D.: Overview of small fixed-wing unmanned aircraft for meteorological sampling, Journal of Atmospheric and Oceanic Technology, 32, 97–115, 2015.

Gerstoft, P. and Hansen, S.: A new tubing system for the measurement of fluctuating pressures, Journal of Wind Engineering and Industrial Aerodynamics, 25, 335 – 354, https://doi.org/https://doi.org/10.1016/0167-6105(87)90026-2, http://www.sciencedirect.com/science/article/pii/0167610587900262, 1987.

365   González-Rocha, J., De Wekker, S. F. J., Ross, S. D., and Woolsey, C. A.: Wind profiling in the lower atmosphere from wind-induced perturbations to multirotor UAS, Sensors, 20, 1341, https://doi.org/10.3390/s20051341, http://arxiv.org/abs/2001.02740https://www.mdpi.com/1424-8220/20/5/1341, 2020.

Hobbs, S., Dyer, D., Courault, D., Olioso, A., Lagouarde, J.-P., Kerr, Y., McAnneney, J., and Bonnefond, J.: Surface layer profiles of air temperature and humidity measured from unmanned aircraft, Agronomie, 22, 635–640, https://doi.org/10.1051/agro:2002050, http://dx.
370   doi.org/10.1051/agro:2002050, 2002.

Illingworth, S., Allen, G., Percival, C., Hollingsworth, P., Gallagher, M., Ricketts, H., Hayes, H., Ładosz, P., Crawley, D., and Roberts, G.: Measurement of boundary layer ozone concentrations on-board a Skywalker unmanned aerial vehicle, Atmospheric Science Letters, pp. n/a–n/a, https://doi.org/10.1002/asl2.496, http://doi.wiley.com/10.1002/asl2.496, 2014.

Jacob, J. D., Chilson, P. B., Houston, A. L., and Smith, S. W.: Considerations for Atmospheric Measurements with Small Unmanned Aircraft
375   Systems, Atmosphere, 9, https://doi.org/10.3390/atmos9070252, http://www.mdpi.com/2073-4433/9/7/252, 2018.

Kral, S., Reuder, J., Vihma, T., Suomi, I., O'Connor, E., Kouznetsov, R., Wrenger, B., Rautenberg, A., Urbancic, G., Jonassen, M., Båserud, L., Maronga, B., Mayer, S., Lorenz, T., Holtslag, A., Steeneveld, G.-J., Seidl, A., Müller, M., Lindenberg, C., Langohr, C., Voss, H., Bange, J., Hundhausen, M., Hilsheimer, P., and Schygulla, M.: Innovative Strategies for Observations in the Arctic Atmospheric Boundary Layer (ISOBAR)—The Hailuoto 2017 Campaign, Atmosphere, 9, 268, https://doi.org/10.3390/atmos9070268, 2018.

380   Laurence, R. J. and Argrow, B. M.: Development and flight test results of a small UAS distributed flush airdata system, Journal of Atmospheric and Oceanic Technology, 35, 1127–1140, https://doi.org/10.1175/JTECH-D-17-0192.1, 2018.

Lenschow, D.: The measurement of air velocity and temperature using the NCAR Buffalo aircraft measuring system, National Center for Atmospheric Research, 1972.

Lenschow, D. and Johnson, W.: Concurrent Airplane and Balloon Measurments of Atmospheric Boundary Layer Structure Over A Forest, J.
385   Appl. Meteor., 7, 79–89, 1968.

Lenschow, D. H.: Airplane Measurements of Planetary Boundary Layer Structure, Journal of Applied Meteorology, 9, 874–884, 1970.

Lothon, M., Lohou, F., Pino, D., Couvreux, F., Pardyjak, E., Reuder, J., Vilà-Guerau De Arellano, J., Durand, P., Hartogensis, O., Legain, D., et al.: The BLLAST field experiment: boundary-layer late afternoon and sunset turbulence, Atmospheric chemistry and physics, 14, 10 931–10 960, 2014.

390   Mansour, M., Kocer, G., Lenherr, C., Chokani, N., and Abhari, R. S.: Seven-Sensor Fast-Response Probe for Full-Scale Wind Turbine Flowfield Measurements, Journal of Engineering for Gas Turbines and Power, 133, https://doi.org/10.1115/1.4002781, https://doi.org/10.1115/1.4002781, 2011.

Parameswaran, V. and Jategaonkar, R. V.: Calibration of 5-hole probe for flow angles from advanced technologies testing aircraft system flight data, Defence Science Journal, 54, 111–123, https://doi.org/10.14429/dsj.54.2073, 2004.

395   Pieri, D., Diaz, J., Bland, G., Fladeland, M., Makel, D., Schwandner, F., Buongiorno, M., and Elston, J.: Unmanned Aerial Technologies for Observations at Active Volcanoes: Advances and Prospects, in: AGU Fall Meeting Abstracts, vol. 2017, pp. NH31A–0204, 2017.

Platis, A., Altstädter, B., Wehner, B., Wildmann, N., Lampert, A., Hermann, M., Birmili, W., and Bange, J.: An Observational Case Study on the Influence of Atmospheric Boundary-Layer Dynamics on New Particle Formation, Boundary-Layer Meteorology, 158, 67–92, https://doi.org/10.1007/s10546-015-0084-y, https://doi.org/10.1007/s10546-015-0084-y, 2016.

400   Ramanathan, V., Ramana, M. V., Roberts, G., Kim, D., Corrigan, C., Chung, C., and Winker, D.: Warming trends in Asia amplified by brown cloud solar absorption, Nature, 448, 575, 2007.

Rautenberg, A., Graf, M. S., Wildmann, N., Platis, A., and Bange, J.: Reviewing wind measurement approaches for fixed-wing unmanned aircraft, Atmosphere, 9, 1–24, https://doi.org/10.3390/atmos9110422, 2018.

Roberts, G. C., Ramana, M. V., Corrigan, C., Kim, D., and Ramanathan, V.: Simultaneous observations of aerosol-cloud-albedo
405   interactions with three stacked unmanned aerial vehicles, Proceedings of the National Academy of Sciences, 105, 7370–7375, https://doi.org/10.1073/pnas.0710308105, http://www.pnas.org/cgi/doi/10.1073/pnas.0710308105, 2008.

Schuyler, T. J. and Guzman, M. I.: Unmanned Aerial Systems for Monitoring Trace Tropospheric Gases, Atmosphere, 8, 206, 2017.

Shevchenko, A. M., Berezin, D. R., Puzirev, L. N., Tarasov, A. Z., Kharitonov, A. M., and Shmakov, A. S.: Multi-hole pressure probes to air data system for subsonic small-scale air vehicles, AIP Conference Proceedings, 1770, https://doi.org/10.1063/1.4963947, 2016.

410   Spiess, T., Bange, J., Buschmann, M., and Vörsmann, P.: First application of the meteorological Mini-UAV 'M2AV', Meteorologische Zeitschrift, 16, 159–169, https://doi.org/10.1127/0941-2948/2007/0195, http://dx.doi.org/10.1127/0941-2948/2007/0195, 2007.

Suomi, I. and Vihma, T.: Wind gust measurement techniques—From traditional anemometry to new possibilities, Sensors (Switzerland), 18, 1–27, https://doi.org/10.3390/s18041300, 2018.

Thomas, R. M., Lehmann, K., Nguyen, H., Jackson, D. L., Wolfe, D., and Ramanathan, V.: Measurement of Turbulent Water Vapor Fluxes
415   Using a Lightweight Unmanned Aerial Vehicle System, Atmos. Meas. Tech, 5, 5529–5568, 2012.

Treaster, A. L. and Yocum, A. M.: The calibration and application of five-hole probes, Tech. rep., DTIC Document, 1978.

van den Kroonenberg, A., Spieß, T., Buschmann, M., Martin, T., Anderson, P., Beyrich, F., and Bange, J.: Boundary layer measurements with the autonomous mini-UAV M^{2}AV, in: Proceedings of DACH2007, Hamburg, Germany, 2007.

Van den Kroonenberg, A., Martin, T., Buschmann, M., Bange, J., and Vörsmann, P.: Measuring the wind vector using the autonomous mini
420   aerial vehicle M2AV, Journal of Atmospheric and Oceanic Technology, 25, 1969–1982, 2008.

Wildmann, N., Rau, G. A., and Bange, J.: Observations of the Early Morning Boundary-Layer Transition with Small Remotely-Piloted Aircraft, Boundary-Layer Meteorology, 157, 345–373, https://doi.org/10.1007/s10546-015-0059-z, https://doi.org/10.1007/s10546-015-0059-z, 2015.

Witte, B. M., Singler, R. F., and Bailey, S. C.: Development of an Unmanned Aerial Vehicle for the Measurement of Turbulence in the
425   Atmospheric Boundary Layer, Atmosphere, 8, 195, 2017.

Yang, H., Sims-Williams, D., and He, L.: Unsteady Pressure Measurement with Correction on Tubing Distortion, in: Unsteady Aerodynamics, Aeroacoustics and Aeroelasticity of Turbomachines, edited by Hall, K. C., Kielb, R. E., and Thomas, J. P., pp. 521–529, Springer Netherlands, Dordrecht, 2006.

Zhou, S., Peng, S., Wang, M., Shen, A., and Liu, Z.: The characteristics and contributing factors of air pollution in Nanjing: A case study based on an unmanned aerial vehicle experiment and multiple datasets, Atmosphere, 9, https://doi.org/10.3390/atmos9090343, 2018.

430